2022

A Low-Order Model for Nonlinear Dynamics of Heat Exchangers

Hongtao Qiao

Christopher Laughman

A Low-Order Model for Nonlinear Dynamics of Heat Exchangers

Hongtao QIAO*, Christopher R. LAUGHMAN

Mitsubishi Electric Research Laboratories
Cambridge, MA 02139
{qiao, laughman}@merl.com

ABSTRACT

This paper proposes a novel low-order heat exchanger modeling approach that possesses the merits of both lumped parameter and moving boundary methods. The dynamics of refrigerant flow are described by the total mass and energy balances across the entire heat exchanger, and the phase transition boundaries are determined by assuming a linear or exponential profile of refrigerant enthalpy distribution. An improved LMTD method is developed to handle temperature crossing. Airside heat transfer is calculated based on a row-by-row analysis. The presented approach owns invariant model structure, resulting in superior numerical robustness. A direct comparison of the proposed model with finite volume and moving boundary methods demonstrates significant improvement over computational speed while the physical integrity is still preserved.

Keywords: dynamic modeling, refrigerant-oil, heat exchanger, lubricant, vapor compression, simulation

1. INTRODUCTION

The construction of high-performance buildings, driven by energy efficiency and sustainability concerns, represents an important trend in the building industry. Energy and comfort requirements for these buildings can result in hygrothermal behavior which is often quite different from buildings constructed using more conventional techniques, due to the reduced air infiltration rates and heat loads. HVAC systems for these buildings must manage ventilation air and the convective and radiative heat and mass transfer processes that affect occupant comfort and health in an energy-efficient manner; this emphasis on energy efficiency in combination with the lower loads combines to motivate the choice of heating, cooling, and ventilation systems that often have design capacities that are lower than conventional systems. Moreover, these systems interact dynamically through the hygrothermal behavior of the space, as all of these systems affect thermal comfort variables of interest, while the system gains for each of these systems are lower due to their smaller design capacities. As a result, high-performance buildings can simultaneously exhibit a wider range of dynamic behavior than conventional buildings, while having less control authority to regulate this behavior.

Well-designed feedback controls are thus necessary to achieve desired energy or comfort objectives and manage dynamic building behavior in the face of disturbances and the lower control authority of the HVAC systems to regulate system variables to their desired setpoints. This need for effective controls for these complex multi-physical systems implies a concomitant need for models that accurately describe the behavior of the individual systems and the interactions between these systems, as such models are an essential tool in designing performant feedback control systems. Physics-based models are perhaps the most popular choice for describing these high-dimensional systems in a design context because their mathematical structure endows them with extrapolative capabilities that are lacking in other modeling formulations, such as time series or neural network-based models.

While these physics-based models have properties that make them well-suited to use in control design problems, HVAC systems for high-performance buildings present several challenges in the construction of accurate models that can be used in an iterative design process. In particular, many of these systems are spatially distributed and described with large sets of numerically stiff nonlinear differential algebraic equations (DAEs) for which simulation over long time horizons is often computationally intensive and takes a substantial amount of wall time. VRF systems, which are increasingly popular because of their superior energy efficiency and installation flexibility as well as temperature control capabilities, exemplify these challenges because they often include tens of indoor units, each of which interacts thermally with each other and with the building envelope. The models for such large-scale HVAC systems thus require management of tradeoffs between accuracy and computational efficiency.

Compared to other components in a typical HVAC system, heat exchangers usually require particular modeling attention, because they are the main components that exchange mass, energy and momentum. It is therefore essential

to obtain accurate mathematical and physical representations for the heat transfer and fluid flow phenomena in heat exchangers. In general, there are three physics-based modeling paradigms for heat exchangers in order of increasing complexity and sophistication (Rasmussen, 2012), i.e., lumped parameter method (LPM), moving boundary method (MBM) and finite volume method (FVM).

Lumped parameter models simplify the description of the characteristics of an inherently spatially distributed physical system with mean properties that are assumed to be homogeneous throughout by averaging out the spatial variations. With this approach, the thermal behavior of heat exchangers is modeled via a single control volume so that there is only one time-varying value for each property, e.g., refrigerant pressure, enthalpy, temperature, or density. The heat transfer between the refrigerant and secondary fluid is evaluated based on the average heat transfer coefficient. These models are often used for early research efforts because of simplicity and computational efficiency. Since they disregard the spatial variation in refrigerant properties and the distinct differences of the heat transfer mechanisms between single-phase and two-phase, these models undoubtedly result in the most inaccurate predictions amongst these three modeling approaches.

In comparison, the moving boundary method is characterized by its division of the heat exchanger into different control volumes, each of which exactly encompasses a particular fluid phase (vapor, two-phase or liquid) and is separated by a moving boundary where phase transition occurs. In contrast to distributed parameter models, the number of control volumes in moving boundary models may vary because fluid phases can disappear or appear under large disturbances. Therefore, this type of model may contain at most three control volumes and at least one at a time. These models are designed to capture the thermal behavior inside these control volumes and time-varying position of phase boundaries. In general, moving boundary models result in much faster simulations than distributed parameter models, but are inherently fragile due to their variable model structure.

Finite volume heat exchanger models are particularly useful for describing spatially dependent phenomena and the detailed component performance, such as the effect of local heat transfer and pressure drops or the branching and joining of refrigerant pipes as a result of particular circuiting configurations. In such models, the governing equations for one-dimensional fluid flow in a form of partial differential equations are spatially discretized and solved by various methods like finite difference, finite volume or finite element methods. While the finite volume method is often chosen because it can accurately maintain conserved quantities, however, this high accuracy is achieved at a cost of longer simulation time. Therefore, model reduction techniques are thus often needed to improve the computational speed.

When it comes to the modeling of large-scale HVAC equipment like VRF systems, the finite volume method is clearly not a preferred choice since the required computational cost is prohibitively expensive. Albeit numerically efficient, the moving boundary method is not in favor either due to its poor robustness. As for the lumped parameter method, its degree of accuracy is a major concern, which hinders the method from being widely used. Consequently, there is a need for a new modeling approach that has good tradeoffs among stability, accuracy and numerical efficiency and can reduce computational cost for simulation of large-scale HVAC systems with complex heat exchanger network. This paper aims to fill the gap by contributing a new modeling approach that possesses the merits of both lumped parameter and moving boundary methods. The remainder of the paper is organized as follows. Section 2 describes the development of the proposed approach. Section 3 presents a direct comparison of the new approach with finite volume and moving boundary models. The conclusions are summarized in Section 4.

2. MODEL DEVELOPMENT

As described previously, each of the three conventional modeling paradigms has its own drawbacks when they are applied to simulate large-scale HVAC systems with complex heat exchanger networks. Hence, the new approach should own the following important traits, (1) low-order and simple, (2) numerically robust, and (3) reasonably accurate so that the model can capture the major fluid flow and heat transfer phenomena. Based on these rationales, the ideal modeling approach for large-scale HVAC systems should have minimum increased complexity over the lumped parameter method, comparable accuracy to and much better robustness than the moving boundary method. As a result, the proposed approach is largely based on the conventional lumped parameter method, but assumes a distribution of refrigerant enthalpy so that the spatial variations of refrigerant properties such as density and specific enthalpy can be taken into account.

The proposed approach relies on the following simplifying assumptions: (1) one-dimensional fluid flow; (2) quasi-steady air flow; (3) negligible refrigerant pressure drop; (4) negligible viscous dissipation; (5) negligible axial conduction in fluid and pipe; (6) negligible kinetic energy and gravitational potential energy; (7) thermodynamic equilibrium for the vapor and liquid in two-phase flows. Based on the assumption (3), the refrigerant side boundary conditions are defined as inlet enthalpy, inlet and outlet mass flow rates.

2.1 Governing Equations: Refrigerant Flow

Similar to the conventional lumped parameter method, the new approach also uses the overall mass and energy balances to describe the dynamics of refrigerant flow.

$$V\frac{d\bar{\rho}}{dt}=\dot{m}_{in}-\dot{m}_{out} \tag{1}$$

$$V\frac{d\left(\overline{\rho u}\right)}{dt}=\dot{m}_{in}h_{in}-\dot{m}_{out}h_{out}+\sum_{j=1}^{3}q_{r,j} \tag{2}$$

where $\bar{\rho}=\frac{1}{V}\int_V \rho dV$ is the mean density of refrigerant in the heat exchanger, where as $\overline{\rho u}=\frac{1}{V}\int_V \rho u dV$ is the mean internal energy of refrigerant in the heat exchanger per unit volume. The subscript *j* on the right side of Eq. (2) is used to denote the flow regimes (vapor, two-phase and liquid) in the heat exchanger.
Given $h=u+p/\rho$, Eq. (2) can be rewritten as

$$V\frac{d\left(\overline{\rho h}\right)}{dt}-V\frac{dp}{dt}=\dot{m}_{in}h_{in}-\dot{m}_{out}h_{out}+\sum_{j=1}^{3}q_{r,j} \tag{3}$$

As we define the mean specific enthalpy as $\bar{h}=\overline{\rho h}/\bar{\rho}=\int_V \rho h dV/\int_V \rho dV$, the overall energy balance of refrigerant flow becomes

$$V\left(\bar{h}\frac{d\bar{\rho}}{dt}+\bar{\rho}\frac{d\bar{h}}{dt}\right)-V\frac{dp}{dt}=\dot{m}_{in}h_{in}-\dot{m}_{out}h_{out}+\sum_{j=1}^{3}q_{r,j} \tag{4}$$

Substituting Eq. (1) into Eq. (4) yields

$$\bar{\rho}V\frac{d\bar{h}}{dt}-V\frac{dp}{dt}=\dot{m}_{in}h_{in}-\dot{m}_{out}h_{out}-\left(\dot{m}_{in}-\dot{m}_{out}\right)\bar{h}+\sum_{j=1}^{3}q_{r,j} \tag{5}$$

Assuming that the mean density $\bar{\rho}$ is a function of pressure *p* and the mean specific enthalpy $\bar{h}$, therefore, Eq. (1) can be expanded into

$$V\left(\frac{\partial\bar{\rho}}{\partial p}\frac{dp}{dt}+\frac{\partial\bar{\rho}}{\partial\bar{h}}\frac{d\bar{h}}{dt}\right)=\dot{m}_{in}-\dot{m}_{out} \tag{6}$$

It can be observed that pressure *p* and the mean specific enthalpy $\bar{h}$ are the dynamic state variables from Eq. (5) and (6). Besides these two state variables, there are two more unknown variables: $\bar{\rho}$ and h_{out}. Remember that $\dot{m}_{\text{in}}$, $\dot{m}_{out}$ and h_{in} are given by the boundary conditions. Therefore, two more relations are needed to have a closed system of equations. One relation comes from the equation of state, i.e., we can calculate $\bar{\rho}$ and its partial derivatives given *p* and $\bar{h}$. The other relation arises from a predefined refrigerant enthalpy distribution profile so that we can compute h_{out}. In the proposed approach, we assume that refrigerant enthalpy varies exponentially in the heat exchanger. Therefore, local refrigerant quality is given by

$$x=\frac{x_{in}-x_{out}}{1-\exp(-1)}\exp(-\zeta)+\frac{x_{out}-x_{in}\exp(-1)}{1-\exp(-1)} \tag{7}$$

where ζ is the fraction of the heat exchanger covered by the portion from the inlet to the location of interest. x_{in} and x_{out} are the refrigerant quality entering and leaving the heat exchanger, respectively. Here refrigerant quality is determined using its extended definition and can be beyond the range of [0, 1], i.e., $x=(h-h_f)/(h_g-h_f)$.
With the enthalpy distribution profile, fractions of vapor, two-phase and liquid zone can be readily computed. Accordingly, the mean specific enthalpy of refrigerant in the heat exchanger can be determined by

$$\bar{h}=\frac{\bar{\rho}_{vap}\bar{h}_{vap}\zeta_{vap}+\left[\bar{\gamma}\rho_g h_g+(1-\bar{\gamma})\rho_f h_f\right]\zeta_{tp}+\bar{\rho}_{liq}\bar{h}_{liq}\zeta_{liq}}{\bar{\rho}} \tag{8}$$

where $\bar{\gamma}$ is the mean void fraction of two-phase. Since $\bar{h}$ is a state variable and is known at each time step, Eq. (8) can be used to iterate h_{out}.

2.2 Improved LMTD Method for Temperature Crossing

LMTD method is used to compute the heat transfer between refrigerant flow and tube wall. Unfortunately, this method fails when there is temperature crossing. A remedy to this issue is to construct a smooth and differentiable function that can extrapolate the LMTD calculation when temperature crossing occurs. Fig. 1 shows seven possible temperature profiles of refrigerant flow and tube walls in the liquid region of a condenser that might occur under transient conditions, and each case is analyzed below.

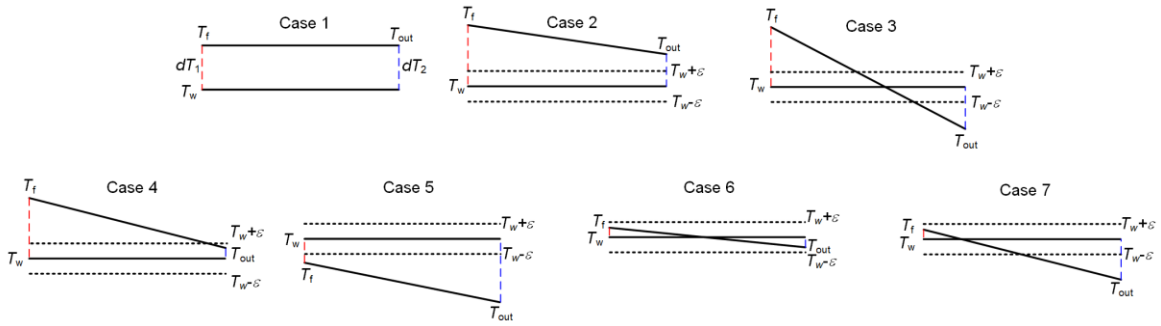

Fig. 1 Temperature profiles between refrigerant flow and tube walls

First of all, let's define

$$dT_1 = T_f - T_w,\ dT_2 = T_{out} - T_w$$

Since T_{out} is always lower than T_f, one can have $dT_1 \geq dT_2$.

Case 1: $\left|dT_1 - dT_2\right| < dT_{\min}$ where $dT_{\min}$ is a very small value, e.g. 1e-6 K.

The original LMTD formulation cannot handle this case because of a possible error of division by zero ($dT_1/dT_2 \approx 1$). As a result, the temperature difference can be determined by

$$\Delta T_{LMTD}\Big|_{(dT_1,dT_2)} = \left(dT_1 + dT_2\right)/2 \tag{9}$$

Case 2: $dT_1 > \varepsilon$ & $dT_2 > \varepsilon$ (ε is a very small positive number, e.g., 1e-6 K)
Case 5: $dT_1 < -\varepsilon$ & $dT_2 < -\varepsilon$
For these two cases, the temperature difference is given by the original formulation.

$$\Delta T_{LMTD}\Big|_{(dT_1,dT_2)} = \left(dT_1 - dT_2\right)/\ln\frac{dT_1}{dT_2} \tag{10}$$

Case 3: $dT_1 > \varepsilon$ & $dT_2 < -\varepsilon$
If dT_1 and dT_2 have different signs, the overall LMTD consists of two parts, i.e., the first part is the temperature difference between dT_1 and $-\varepsilon$, and the second part is the temperature difference between $-\varepsilon$ and dT_2. For the first part, the original LMTD equation cannot be used because of the negative temperature difference. Instead, one needs to first calculate the LMTD between dT_1 and ε, and then linearly extrapolate the calculation to obtain the LMTD between dT_1 and $-\varepsilon$. The second part can be directly calculated using the original LMTD equation. The overall LMTD is the weighted sum of two parts.

$$\Delta T_{LMTD}\Big|_{(dT_1,dT_2)} = \frac{\left|dT_1+\varepsilon\right|}{\left|dT_1\right|+\left|dT_2\right|}\left[\Delta T_{LMTD}\Big|_{(dT_1,\varepsilon)} - 2\varepsilon\left.\frac{\partial\left(\Delta T_{LMTD}\right)}{\partial\left(dT_2\right)}\right|_{dT_2=\varepsilon}\right] + \left(1-\frac{\left|dT_1+\varepsilon\right|}{\left|dT_1\right|+\left|dT_2\right|}\right)\Delta T_{LMTD}\Big|_{(-\varepsilon,dT_2)} \tag{11}$$

where

$$\Delta T_{LMTD}\big|_{(dT_1,\varepsilon)} = \left(dT_1 - \varepsilon\right) / \ln\frac{dT_1}{\varepsilon} \tag{12}$$

$$\Delta T_{LMTD}\big|_{(-\varepsilon,dT_2)} = -\left(\varepsilon + dT_2\right) / \ln\frac{-\varepsilon}{dT_2} \tag{13}$$

$$\left.\frac{\partial\left(\Delta T_{LMTD}\right)}{\partial\left(dT_2\right)}\right|_{dT_2=\varepsilon} = 1/\ln\frac{\varepsilon}{dT_1} - \left(1-\frac{dT_1}{\varepsilon}\right)/\left(\ln\frac{\varepsilon}{dT_1}\right)^2 \tag{14}$$

Case 4: $dT_1 > \varepsilon$ & $-\varepsilon < dT_2 < \varepsilon$
The overall LMTD is calculated by extrapolation

$$\Delta T_{LMTD}\big|_{(dT_1,dT_2)} = \Delta T_{LMTD}\big|_{(dT_1,\varepsilon)} + \left(dT_2 - \varepsilon\right)\left.\frac{\partial\left(\Delta T_{LMTD}\right)}{\partial\left(dT_2\right)}\right|_{dT_2=\varepsilon} \tag{15}$$

where $\Delta T_{LMTD}\big|_{(dT_1,\varepsilon)}$ is calculated by Eq. (10).

Case 6: $-\varepsilon \le dT_1 \le \varepsilon$ & $-\varepsilon \le dT_2 \le \varepsilon$
The overall LMTD is

$$\Delta T_{LMTD}\big|_{(dT_1,dT_2)} = \left(dT_1 + dT_2\right)/2 \tag{16}$$

Case 7: $-\varepsilon < dT_1 < \varepsilon$ & $dT_2 \le -\varepsilon$
This case is similar to Case 4, and the overall LMTD is calculated by interpolation

$$\Delta T_{LMTD}\big|_{(dT_1,dT_2)} = \Delta T_{LMTD}\big|_{(-\varepsilon,dT_2)} + \left(dT_1 + \varepsilon\right)\left.\frac{\partial\left(\Delta T_{LMTD}\right)}{\partial\left(dT_1\right)}\right|_{dT_1=-\varepsilon} \tag{17}$$

$$\left.\frac{\partial\left(\Delta T_{LMTD}\right)}{\partial\left(dT_1\right)}\right|_{dT_1=-\varepsilon} = 1/\ln\frac{-\varepsilon}{dT_2} - \left(1+\frac{dT_2}{\varepsilon}\right)/\left(\ln\frac{-\varepsilon}{dT_2}\right)^2 \tag{18}$$

where $\Delta T_{LMTD}\big|_{(-\varepsilon,dT_2)}$ is obtained via Eq. (10).

2.3 Governing Equations: Air Flow

For the calculation of air side heat transfer, a row-by-row analysis is used in the proposed approach, i.e., heat transfer is evaluated for the tubes in a given row based on the refrigerant parameters in the individual tubes and the average air temperature/humidity leaving the preceding row such that the non-uniformity of the air parameters along the flow direction can be retained. Although this row-by-row analysis neglects the non-uniformity of the air parameters on the plane perpendicular to the direction of airflow, it does not cause substantial deviations in the prediction because the degree of this non-uniformity tends to be small. To perform such a row-by-row analysis, the following rules are proposed to obtain a more reasonable simplification for multi-row coils (the rules are also applicable for single-row coils):

Rule 1 - The coil is simplified to be a single-circuit coil with both refrigerant mass flow rate and air flow rate reduced by a factor of $1/N_{cir}$, where N_{cir} is the number of coil circuits (in Fig. 2, N_{cir} is equal to 3).

Rule 2 - The simplified coil is an N_{row} pass coil with N_{row} horizontal tubes, where N_{row} is the number of rows in the original coil (in Fig. 2, N_{row} is equal to 3).

Rule 3 - The new tube length in the simplified coil is $N_t L_t/(N_{cir}N_{row})$, where L_t and N_t are the tube length and the total number of tubes in the original coil, respectively (in Fig. 2, N_t is equal to 78).

Rule 4 - The simplified coil needs to retain the same flow configuration as the original coil, i.e., parallel or counter flow (parallel flow for the coil in Fig. 2).

Following the above rules, the coil in Fig. 2 can be simplified as a single-circuit, three-pass coil with parallel flow configuration. The tube length is 78/9 times its original length. Both refrigerant mass flow rate and air flow rate are reduced to one third of their original values.

With the above simplification rules, the air flow propagation can be taken into account in the analysis. As a result, heat transfer for each tube in the simplified coil needs to be evaluated. In order to separately calculate the heat transfer between air flow and each tube in the simplified coil, the percentage of each tube contributing to each zone needs to be computed first.

Tubes in the simplified coil are numbered starting from the refrigerant inlet, following the refrigerant flow direction until the outlet is reached, i.e., the refrigerant inlet is the first tube and the refrigerant outlet is the last tube. For the parallel flow configuration coil, the first tube gets the fresh air, whereas for the counter flow coil, the last tube gets the fresh air.

The fraction of the i^{th} tube covered by Zone 1 (vapor zone for the condenser or liquid zone for the evaporator) is

$$\beta_1^i = \min\left[1, \max\left(0, \zeta_1 N_{row} - i + 1\right)\right] \tag{19}$$

where ζ_1 is the fraction of the total heat exchanger length covered by Zone 1. The superscript "i" denotes the i^{th} tube.

The fraction of the i^{th} tube covered by Zone 2 (two-phase zone) is

$$\beta_2^i = \min\left[1, \max\left(0, \zeta_1 N_{row} + \zeta_2 N_{row} - i + 1\right)\right] - \beta_1^i \tag{20}$$

where ζ_2 is the fraction of the total heat exchanger length covered by Zone 2.

The fraction of the i^{th} tube covered by Zone 3 (liquid zone for condenser or vapor zone for evaporator) is

$$\beta_3^i = 1 - \beta_2^i - \beta_1^i \tag{21}$$

The sensible heat transfer between the air stream and the portion of the i^{th} tube covered by Zone j is

$$q_{dry,j}^i = \dot{m}_a c_{p,a} \beta_j^i \left(T_a^i - T_{w,j}\right)\left[1 - \exp\left(-\frac{\alpha_a A_{o,eff}}{\dot{m}_a c_{p,a} N_{row}}\right)\right] \tag{22}$$

where $\dot{m}_a$ is the air mass flow rate in the simplified coil, T_a^i is the air temperature entering the i^{th} tube, and $A_{o,eff}$ is the total effective surface area of the simplified coil.

The latent heat transfer between the air stream and the portion of the i^{th} tube covered by Zone j is

$$q_{wet,j}^i = \dot{m}_a \beta_j^i \max\left(0, \omega_a^i - \omega_{a,sat,j}\right) \Delta h_{fg,j}\left[1 - \exp\left(-\frac{\alpha_a A_{o,eff}}{\dot{m}_a c_{p,a} Le^{2/3} N_{row}}\right)\right] \tag{23}$$

where ω_a^i is the air inlet humidity ratio of the i^{th} tube, $\omega_{a,sat,j}$ is the humidity ratio of saturated moist air evaluated at $T_{w,j}$, and $\Delta h_{fg,j}$ is the latent heat of water vapor at $T_{w,j}$.

The water condensate flow rate that occurs on the portion of i^{th} tube covered by Zone j is

$$\dot{m}_{water,j}^i = \dot{m}_a \beta_j^i \max\left(0, \omega_a^i - \omega_{a,sat,j}\right)\left[1 - \exp\left(-\frac{\alpha_a A_{o,eff}}{\dot{m}_a c_{p,a} Le^{2/3} N_{row}}\right)\right] \tag{24}$$

Therefore, air-to-wall heat transfer for Zone j is

$$q_{a,j} = \sum_{i=1}^{N_{row}} \left(q_{dry,j}^i + q_{wet,j}^i\right) \tag{25}$$

The air-to-wall heat transfer for the i^{th} tube is

$$q_a^i = \sum_{j=1}^{3} \left(q_{dry,j}^i + q_{wet,j}^i\right) \tag{26}$$

Energy balance for the air stream across each tube needs to be considered to solve the air state at the intermediate tubes. For the parallel flow configuration, h_a^1 and ω_a^1 are known as the inlet conditions, whereas $h_a^{N_{row}+1}$ and $\omega_a^{N_{row}+1}$ are solved as the outlet conditions. For the counter flow configuration, $h_a^{N_{row}}$ and $\omega_a^{N_{row}}$ are known as the inlet conditions, while h_a^0 and ω_a^0 are solved as the outlet conditions.

Parallel flow configuration

$$\dot{m}_a(h_a^i - h_a^{i+1}) = q_a^i + \sum_{j=1}^{3}\left(\dot{m}_{water,j}^i h_{water,j}\right) \tag{27}$$

$$\dot{m}_a(\omega_a^i - \omega_a^{i+1}) = \sum_{j=1}^{3}\dot{m}_{water,j}^i \tag{28}$$

Counter flow configuration

$$\dot{m}_a(h_a^i - h_a^{i-1}) = q_a^i + \sum_{j=1}^{3}\left(\dot{m}_{water,j}^i h_{water,j}\right) \tag{29}$$

$$\dot{m}_a(\omega_a^i - \omega_a^{i-1}) = \sum_{j=1}^{3}\dot{m}_{water,j}^i \tag{30}$$

2.4 Governing Equations: Tube Walls

The energy balance equation for the tube walls in each of the active zones can be written as

$$\frac{dT_{w,j}}{dt} = \frac{q_{a,j} - q_{r,j}}{C_w L_j} \tag{31}$$

where C_w is the combined heat capacity of tube and fins per unit length. When a zone is inactive, Eq. (31) is replaced by a pseudo-state equation to track the tube wall temperature in the adjacent active zone.

3. RESULTS AND DISCUSSIONS

The proposed approach was used to develop a dynamic model of a multi-split air-source air-conditioning system with a separate evaporator located in each indoor space, as illustrated in Fig. 3 and briefly described here. As is the case in most vapor compression cycles, the discharge gas leaving the compressor first flows into the outdoor heat exchanger, where it condenses to a liquid. This condensed refrigerant then passes through a first expansion valve (LEVM) and into a high-side receiver, after which it splits into a manifold that connects to each of the four indoor units. The refrigerant in each individual line then is further expanded through an additional expansion valve, which typically has a much smaller orifice size than LEVM, and then flows through adiabatic refrigerant pipes. The refrigerant in each line then enters the indoor heat exchanger, where it evaporates and returns to the outdoor unit through another set of long pipes to a manifold that connects to the suction port of the compressor. Standard tube-fin heat exchangers were used for both the condenser and evaporators, as well as a rotary compressor and electronic expansion valves with a nearly linear response (LEV). Details for other component models of the multi-zone vapor-compression system are provided in Qiao et al. (2017).

A number of geometric and fluid parameters were required to configure the air-source air-conditioner; particularly important quantities are provided in Table 1. Each indoor unit multi-zone system had a nominal cooling capacity of 1136 W sensible and 856 W latent at a compressor frequency of 55 Hz, with 3 °C of condenser subcooling when each indoor zone was at 23.5 °C and 4.6 °C of superheat in each evaporator when the ambient environment was at 27.2 °C. The building models were based upon the open-source Modelica Buildings library (Wetter et al., 2014), an extensive and well-tested library of components for the construction of dynamic building system models. The room model from the Buildings library are based on the physics-based behavior of the fundamental materials and components commonly used in the building construction industry. These individual materials are parameterized by fundamental properties like thickness, thermal conductivity, and density, and can be combined and assembled into multi-layer constructions. The accuracy of the multi-layer models is ensured by automating the discretization of the partial differential equations representing heat transfer in the materials by using the Fourier number to ensure that the time constants of each volume are approximately equal. The zone air model is a mixed air single-node model with one bulk air temperature that interacts with all of the radiative surfaces and thermal loads in the room, where the zone is assumed to have convective, radiative, and latent gains specified on a per area basis. The radiative heat transfer representing the solar heat gains and the infrared heat transfer between the interior surfaces of the room are also described by characterizing the absorptivity and emissivity of each surface, which is used with a set of simplified view factors between the surfaces in the room as an approximation to avoid the complexity of incorporating the detailed room geometries.

This building was located in Chicago, IL, USA, and the corresponding TMY3 weather file was used to drive the model with realistic solar and thermal boundary conditions to understand the detailed room thermal dynamics. Each space was assumed to contain 17 W/m^2 of latent load and 60 W/m^2 of sensible load. The cycle and building models were assembled into an overall system model and simulated eight-hour operation from 9:00 am to 5:00 pm on July 19th to evaluate its system performance.

These models were implemented in the Modelica language using the Dymola 2020x simulation environment (AB Dassault Systemes, 2020), while the refrigerant property models for R-410A were obtained using the pseudo-pure formulation (Lemmon, 2003). These models were compiled and run on a laptop with an Intel i7 processor with 32 Gb of RAM; the DASSL solver was used to integrate the set of differential algebraic equations with a tolerance of 10^{-5}.

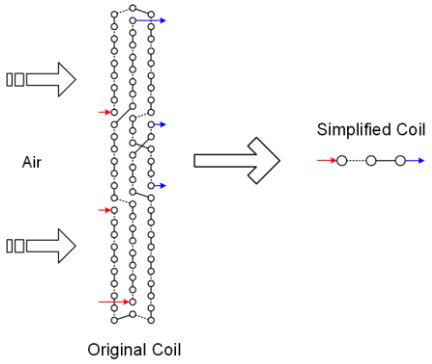

Fig. 2 Simplification of multi-row coils

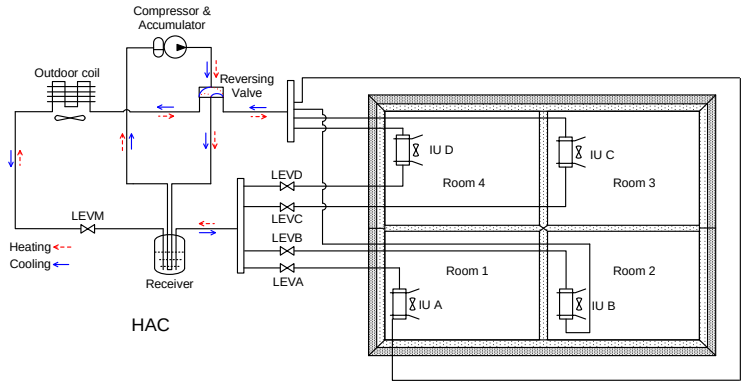

Fig. 3 Building with four conditioned zones served by a multi-split AC

Table 1. Heat exchanger geometric parameters

Parameters	Value
Refrigerant	R410A
OU HEX tube diameter	9.5 mm
IU HEX tube diameter	7 mm
OU HEX tube length	0.77 m
IU HEX tube length	0.63 m
OU HEX number of tubes	64
IU HEX number of tubes	32

A direct comparison of pull-down simulation was conducted between the proposed approach and the moving boundary (Qiao et al., 2016) and finite volume methods (Qiao et al., 2015) on the system dynamics and prediction accuracy as well as simulation speed to evaluate its efficacy. Statistics with different modeling methods were given in Table 2. It is evident that the new method resulted in a model with significantly lower order (45th order) comparing with FVM (363rd order) and the MBM (88th order). As a result, the simulation speed was improved substantially in the presented study, around 60 times and 3.5 times faster, respectively. Savings potential for computational costs can be enormous for the large-scale VRF systems with tens of indoor units.

Fig. 4 showed the comparison for simulation results with these three methods (all rooms were identical and only the air temperature in room 1 was shown). It can observed that the results obtained by the new method agreed reasonably well with the other two more sophisticated methods. The large deviations of the heat load prediction for both indoor and outdoor coils were observed at the beginning (Fig. 4c and 4d) because refrigerant enthalpy distribution was initialized differently (exponential profile for the new method, linear profile for the other two methods). Fig. 4e and 4f illustrated the fraction of each zone for both outdoor and indoor coils calculated by the new method. This confirmed that the new method was able to track the phase boundaries like MBM. However, only two differential equations were needed for the new method, whereas six was needed for MBM. More importantly, switching schemes were not required to handle the case with changing number of fluid phases in the new method because of its invariant model structure. From these comparisons, it was convincing that the new method had a good tradeoff between numerical efficiency, accuracy and robustness.

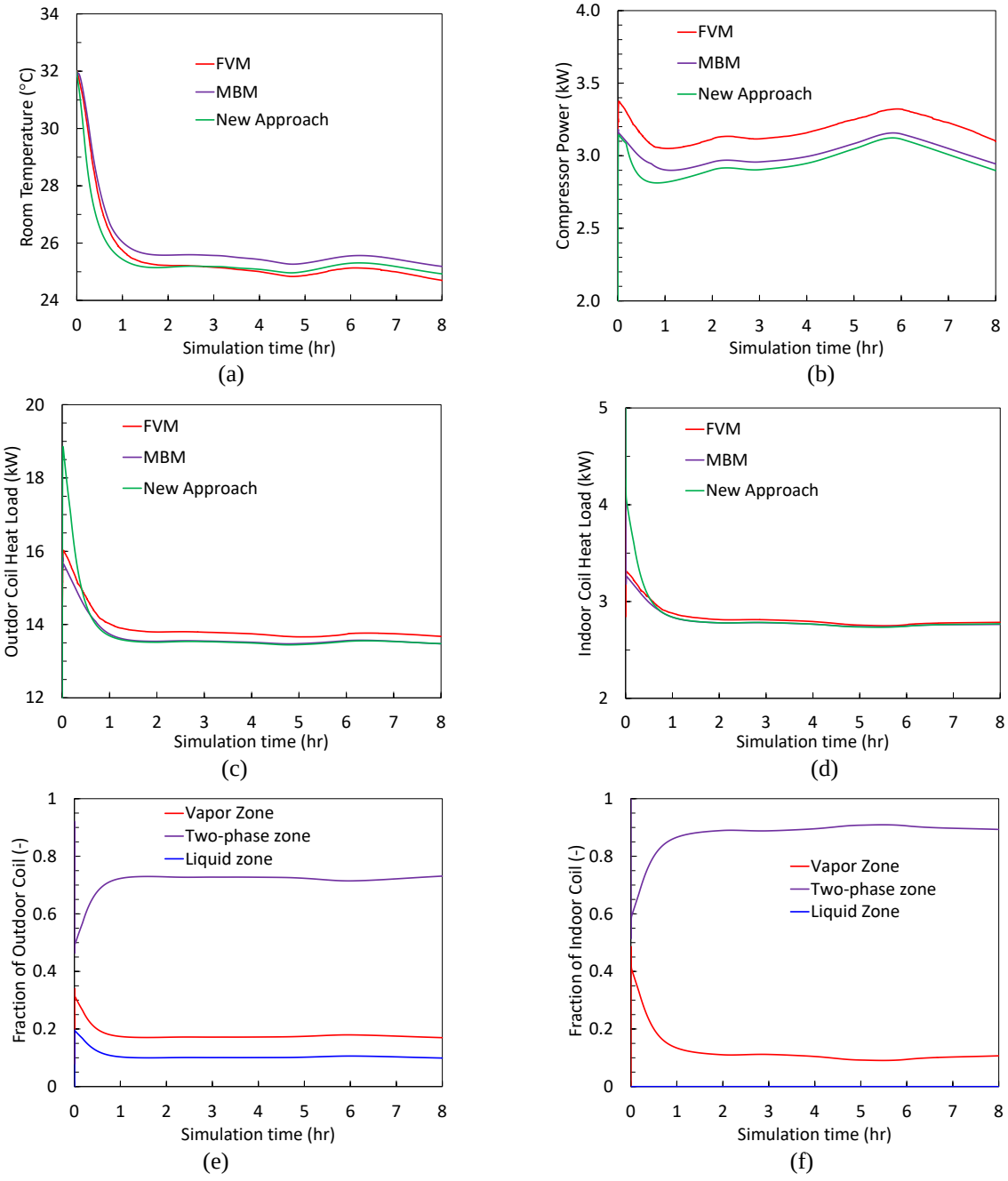

Fig. 4 Pull-down simulation results: (a) air temperature transients in room 1; (b) compressor power; (c) outdoor coil heat load; (d) indoor coil heat load; (e) outdoor coil breakdown by the new approach; (f) indoor coil breakdown by the new approach

Table 2. Model statistics

Parameters	FVM	MBM	Proposed Approach
number of equations	24417	3216	2488
number of continuous time states	363	88	45
number of numerical Jacobians	5	0	0
CPU time (sec)	981	58	16

4. CONCLUSIONS

This work presented an effective approach for simulating the dynamic behavior of large-scale HVAC systems with complex heat exchanger networks. The complexity level of heat exchanger models was found to be essential, as it imposed significant impact on the computational costs of simulations. Meanwhile, numerical robustness was another important aspect that was worth great attention in model development. Further work to refine this approach for performing simulations under zero flow conditions and the design of control architectures will be valuable in improving the energy efficiency of high performance buildings.

NOMENCLATURE

Symbols		***Subscripts***	
A	area	a	air
C	capacitance	dry	dry condition value
c_p	specific heat	eff	effective
h	specific enthalpy	f	fluid
L	length	g	gas
Le	Lewis number	in	inlet
$\dot{m}$	mass flow rate	liq	liquid
p	pressure	o	external
q	heat transfer rate	out	outlet
T	temperature	sat	saturation
u	specific internal energy	r	refrigerant
V	volume	t	tube
x	quality	tp	two-phase
α	heat transfer coefficient	vap	vapor
γ	void fraction	w	tube wall
ρ	density	wet	wet condition
ω	humidity ratio		

REFERENCES

AB Dassault Systemes. Dymola 2020.

Lemmon EW. Pseudo-pure fluid equations of state for the refrigerant blends R-410A, R404A, R507A, and R-407C. *Int. J. Thermophys.* 2003; 24: 991-1006.

Qiao, H., Aute, V., Radermacher, R., 2015. Transient modeling of a flash tank vapor injection heat pump system - Part I: Model development. *Int. J. Refrigeration* 49, 169-182.

Qiao, H., Laughman, C.R., Aute, V., Radermacher, R., 2016. An advanced switching moving boundary heat exchanger model with pressure drop. *Int. J. Refrigeration* 65, 154-171.

Qiao, H., Laughman, C.R., Burns, D., Bortoff, S., 2017. Dynamic characteristics of an R410-A multi-split variable refrigerant flow air-conditioning system. 12th IEA Heat Pump Conference, Rotterdam, Netherlands.

Rasmussen, B., 2012. Dynamic modeling for vapor compression systems-Part I: Literature review. *HVAC&R Res.* 18, 934-955.

Wetter, M., Zuo, W., Nouidui, T.S., Pang, X., 2014. Modelica Buildings Library. *J. Build. Perform. Simu*. 7, 253-270.